Phys Chem Minerals (2003) 30: 449–456
DOI 10.1007/s00269-003-0322-6

ORIGINAL PAPER

A. Suzuki · E. Ohtani

Density of peridotite melts at high pressure

Received: 7 May 2002 / Accepted: 24 April 2003

Abstract Densities of ultramafic melts were determined up to 22 GPa by relative buoyancy experiments. Olivine and diamond were used as buoyancy markers. We confirmed that the density crossover of PHN 1611 melt and its equilibrium olivine (Fo94) occurs at around 13.5 GPa and 2030 °C and that olivine floats from deeper regions in the magma ocean of the primordial terrestrial mantle. The comparison of the compression curves of basic and ultrabasic melts implies that the basic melt is more compressible. This can be explained by the difference in the amount of compressible linkage of SiO_n and AlO_n polyhedra. The interstitial melt trapped by the density crossover can be the cause of the impedance anomaly of the seismic wave in the deep upper mantle.

Keywords Density · Magma · Magma ocean · High pressure · Differentiation · Mantle · Silicate melt

Introduction

The density of silicate melt has played an important role in the differentiation of the terrestrial planets. Numerical simulations suggest that the uppermost region of the terrestrial planets melted globally in the earliest stage of formation (e.g., Hayashi et al. 1979; Kaula 1979; Abe and Matsui 1985; Sasaki and Nakazawa 1986; Melosh 1990). Metal/silicate partitioning experiments also support the existence of a deep magma ocean (e.g., Li and Agee 1996, 2001; Ohtani et al. 1997). Therefore, chemical differentiation in the planetary interior is thought to occur by the fractionation of minerals in the magma ocean. Using the estimation and the preliminary measurement of density of silicate melt at high pressure, it has also been suggested that the density crossover between the mantle melt and the equilibrium minerals could have produced a stratified mantle (Ohtani 1983, 1985, 1988; Agee and Walker 1988a,b; Miller et al. 1991a). High-temperature conditions in the earliest Earth are suggested by the existence of komatiite, which is an ultrabasic igneous rock found in the Archean. The deep origin of komatiites has been explained by the density relation between komatiite magma and the surrounding mantle (Nisbet and Walker 1982; Ohtani 1984, 1990; Miller et al. 1991b).

Density measurements of silicate melts have been carried out in order to constrain the early differentiation processes in the Earth and planetary interiors (e.g., Agee and Walker 1988a, 1993; Miller et al. 1991b; Ohtani et al. 1993, 1998; Suzuki et al. 1995, 1998). Although the density crossover of the Martian mantle melt and the equilibrium olivine was reported (Ohtani et al. 1993; Suzuki et al. 1998), the density relation between olivine and terrestrial mantle melts has not been confirmed. Agee and Walker (1988a) measured the density of an aluminum-undepleted komatiite (AUK) and a peridotite KLB-1 melt by observing the sinking and flotation of olivine under static compression up to 6 GPa. However, chemical compositions were modified by mixing fayalite (Fe_2SiO_4) up to 50% in order to observe the flotation of olivine within the pressure range of their experiment. Agee and Walker (1993) later used a multianvil apparatus to extend the pressure range of density measurement. Flotation of forsterite (Fo100) was observed at 9.1 GPa and 2000 °C in KLB-1 melt. However, since San Carlos olivine (Fo90) sank to 11.1 GPa, they could not confirm the density crossover of KLB-1 melt and the equilibrium olivine. Ohtani et al. (1998) showed preliminary results of a buoyancy test using PHN 1611 melt and its equilibrium olivine, and demonstrated the sinking of olivine in the melt to 12 GPa. They observed only sinking of olivine, and the pressures in their experiments were estimated based on the preliminary pressure calibration curve. In the present study, the density crossover

A. Suzuki (✉) · E. Ohtani
Institute of Mineralogy Petrology and Economic Geology, Faculty of Science, Tohoku University, Sendai 980–8578, Japan
e-mail: a-suzuki@mail.cc.tohoku.ac.jp

Present addres: A. Suzuki
Bayerisches Geoinstitut, Universität Bayreuth, 95440 Bayreuth, Germany

between PHN1611 melt and the equilibrium olivine has been observed. Density measurements of the peridotitic melts have been also carried out to 22 GPa using diamond as a buoyancy marker.

Experimental

We employed three ultrabasic silicate compositions, which were based on a primitive peridotite PHN1611 (Nixon and Boyd 1973), pyrolite (Ringwood 1975), and a primitive peridotite (Jagoutz et al. 1979). The original compositions were simplified to five components in the CaO–FeO–MgO–Al_2O_3–SiO_2 system (Table 1). O'Hara's method of simplification (O'Hara 1975) was applied to convert from multicomponent to CMAS (CaO–MgO–Al_2O_3–SiO_2) system from the original composition of primitive peridotite by Jagoutz et al. (1979). Then a five-component mixture was calculated, in which the ratio of FeO/MgO was the same as the original composition. We named this composition JPP (Table 1). We synthesized the starting material by mixing reagents of MgO (99.0% pure), Fe_2O_3 (99.5% pure), Al_2O_3 (99.5% pure), SiO_2 (99.9% pure), and $CaCO_3$ (99.9% pure). After sufficiently mixed and ground, the powder was crystallized at 1100 °C by controlling the oxygen fugacity at $\log f_{O2} = 10^{-12}$ for 20 h. The synthesized materials consisted of olivine, orthopyroxene, clinopyroxene, and anorthite.

Pressure was generated by using a Kawai-type (MA-8) multianvil apparatus installed at Tohoku University (Kawai and Endo 1970; Kawai et al. 1973; Onodera 1987). Two types of pressure cell assemblies were employed for the experiments. Edge lengths of the octahedral pressure medium were 9.65 and 13.15 mm. The former cell and its pressure calibration have been described in a previous work (Suzuki et al. 1998). A cross-section of the cell with 13.15-mm edge length is drawn in Fig. 1. Toshiba F-grade tungsten carbide cubes with truncated edge length (TEL) of 7.0 mm were used for this pressure cell. The 7.0/13.15 system was used to 13.9 GPa (Table 2). A lanthanum chromite heater was used in the furnace. A sample container was made of graphite. The temperature was measured by a $W_{97}Re_3$–$W_{75}Re_{25}$ thermocouple, and the pressure effect on emf was not considered. The pressure of experiments with a 7.0/13.15 system (Fig. 2) was calibrated using the fixed points of the α–β transition of Mg_2SiO_4 (Morishima et al. 1994) the garnet-perovskite transition of $CaGeO_3$ (Susaki et al. 1985), and the coesite–stishovite transition (Liu et al. 1996). The experiments of pressure calibration were carried out at intervals of 20 tons. The pressure of the run condition was estimated from the calibration curve at 1800 °C (Table 2). The curve at 1200 °C was used to

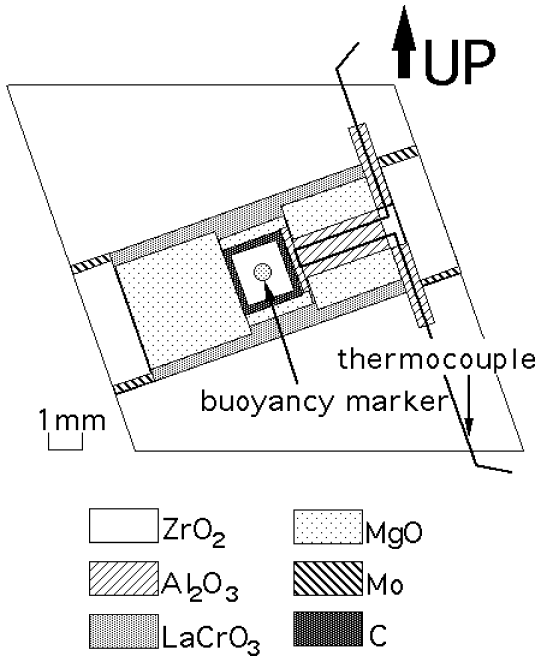

Fig. 1 Pressure cell assembly (7.0/13.15 system) for density measurement. This assembly was used for the density measurement of the PHN1611 melt up to 13.9 GPa. We used the 3.5/9.65 system over 14.2 GPa. The detail of the assembly and the pressure calibration were already described in Suzuki et al. (1998)

Table 1 Chemical compositions of starting materials

	PHN1611[a]	Pyrolite[b]	JPP[c]	MA[d]	KLB-1[e]	MORB[f]
SiO_2	45.1	46.2	44.4	42.1	44.48	51.81
TiO_2	–	–	–	–	0.16	–
Al_2O_3	2.8	3.6	5.1	6.5	3.59	15.95
Cr_2O_3	–	–	–	–	0.31	–
FeO	10.4	8.7	8.2	16.0	8.10	9.97
MnO	–	–	–	–	0.12	–
MgO	38.4	38.3	38.2	30.2	39.22	7.86
CaO	3.4	3.2	4.1	5.3	3.44	11.69
Na_2O	–	–	–	–	0.30	2.72
K_2O	–	–	–	–	0.02	–
P_2O_5	–	–	–	–	0.03	–
NiO	–	–	–	–	0.25	–
Total (wt%)	100.0	100.0	100.0	100.0	100.02	100.00
Mg#	86.9	88.7	89.3	77.1	89.6	58.4
Mg#(ol)	94.5	95.4	95.6	89.9	95.8	78.7

Mg# = MgO/(MgO + FeO) × 100, molar
Mg#(ol) is the composition of olivine, which is in equilibrium with melt. $K_D = (MgO/FeO)_{ol}/(MgO/FeO)_{melt} = 0.38$ is assumed
[a] Garnet lherzolite (Nixon and Boyd 1973)
[b] Model composition of terrestrial mantle (Ringwood 1975)
[c] Primitive peridotite (Jagoutz et al. 1979)
[d] Model composition of Martian mantle (Morgan and Anders 1979)
[e] Spinel lherzolite, KLB-1 (Takahashi 1986)
[f] Mid-ocean ridge basalt (Yasuda et al. 1994)

Table 2 Experimental conditions and results. Errors in temperature are based on the fluctuation during heating

Run	Pressure (GPa)	Temperature (°C)	Time (s)	Buoyancy marker	Result
PHN1611 melt					
PHN-03	7.0	2000 ± 100	30	c-BN	Sink
PHN-04	7.0	1920 ± 40	20	c-BN	Sink
PHN-14	10.6	1870 ± 20	10	Ol (Fo94)	Sink
PHN-17	12.3	1950 ± 20	20	Ol (Fo94)	Sink
PHN-27	13.5	2040 ± 10	2	Ol (Fo94)	Neutral
PHN-19	13.5	2030 ± 30	11	Ol (Fo94)	Neutral
PHN-21	13.9	1980 ± 10	2	Ol (Fo94)	Float
PHN-06	15.0	2400 ± 50	40	Diamond	Sink
PHN-10[a]	20.2	2360[b]	300	Diamond	Sink
PHN-12[a]	20.7	2360[b]	300	Diamond	Float
PHN-11[a]	21.2	2360[b]	300	Diamond	Float
PHN-08[a]	22.1	2360[b]	300	Diamond	Float
Pyrolite melt					
PYR-5[c]	8.1	1985 ± 20	60	Ol(Fo94)	Sink
PYR-94[c]	10.3	2000 ± 100	120	Ol(Fo94)	Sink
PYR-30	22.1	2360[b]	300	Diamond	Neutral
Primitive peridotite melt					
JPP-02	14.2	2320[b]	180	Diamond	Sink
JPP-04	18.0	2220[b]	170	Diamond	Sink
JPP-07	20.4	2500[b]	200	Diamond	Sink
JPP-08	20.4	2360[b]	360	Diamond	Sink
JPP-12	22.1	2360[b]	300	Diamond	Sink

[a] Results from Suzuki et al. (1995)
[b] Temperature was estimated from electric power
[c] Results from Ohtani et al. (1993, 1995). Pressure was corrected using the revised calibration curve

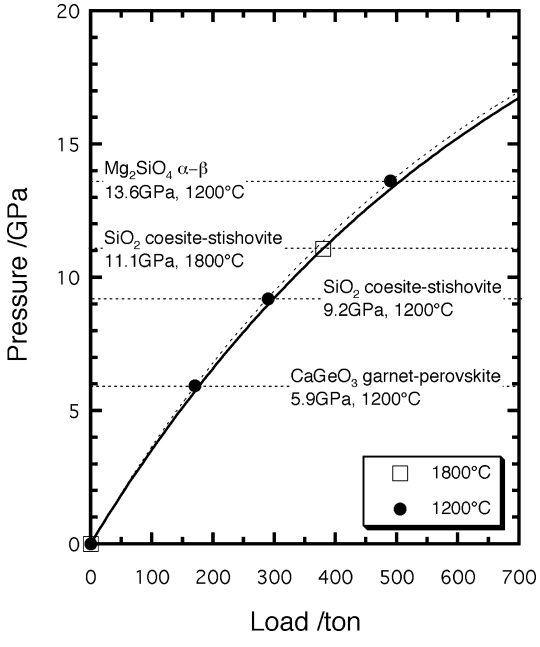

Fig. 2 Pressure calibration curve of 7.0/13.15 system. The experiments were carried out at every 20 tons to determine the phase boundaries. The synthesized phase was identified by using X-ray diffraction data. We adopted the pressure calibration curve at 1800 °C to estimate the run conditions

estimate the curvature of 1800 °C. The accuracy of pressure is estimated to be ± 0.3 GPa based on the run intervals of calibration and the accuracy of the fixed point. All the ceramic parts were heated at 700 °C for over 12 h in order to remove water, and the assembled run charges were then stored in an oven at 130 °C.

The density measurement of the melts was conducted by observing the sinking and flotation of a crystal (buoyancy marker). Olivine in a peridotite xenolith from Bultfontein Mine (Fo94, K. Aoki, personal communication), single crystalline diamond, and polycrystalline cubic boron nitride were used as buoyancy markers. Thermoelastic parameters of buoyancy markers have been described in a previous paper (Suzuki et al. 1995, 1998). Data for cubic boron nitride are from Knittle et al. (1989). Initially, a buoyancy marker was loaded in the center of the container. A charge was compressed at first to the desired pressure, and then heated to about 100 °C below the solidus within several minutes. In order to avoid dissolution of the olivine, the temperature was elevated quickly (about 50 $°Cs^{-1}$) to the desired value, which is about 10 to 50 °C higher than the liquidus, and maintained for several seconds. In the experiments in which a diamond crystal was used as a buoyancy marker, the heating duration was about 5 min. Temperature was dropped by cutting off the electric power supply. The recovered charge was cut and observed under a microscope. The scanning electron microscope (SEM) was also used to observe the charge, and the EPMA was used to measure the chemical compositions.

Results and discussion

The experimental conditions and results are shown in Table 2. The zero-pressure densities of melts are calculated by using partial molar volumes of oxide components in silicate liquid (Lange and Carmichael 1987, 1990). In some runs, temperatures were estimated by the extrapolation of the relation between electric power and temperature, because thermocouples were damaged between 1500 and 1800 °C. The uncertainties in the estimated temperatures are ± 100 °C based on the power–temperature relation up to the temperature where the thermocouples were damaged. We observed

sinking of cubic boron nitride at 7.0 GPa in the PHN1611 melt. The buoyancy tests with an olivine marker were conducted up to 13.9 GPa and 2040 °C. The present study confirms that the equilibrium olivine (Fo94) sinks in PHN 1611 melt up to 12.3 GPa and 1950 °C, and is neutrally buoyant at 13.5 GPa. The density crossover of olivine and PHN1611 melt exists around 13.5 GPa, and olivine floats at 13.9 GPa and 1980 °C. Figure 3a is a photomicrograph of the run PHN-17 which reveals that olivine (Fo94) sank in the PHN1611 melt at 12.3 GPa and 1950 °C, The runs PHN-19 (Fig. 3b) and –27 show the neutral buoyancy of olivine (Fo94) at 13.5 GPa, because olivine did not move during two different heating durations. In the run PHN-21 (Fig. 3c), the equilibrium olivine (Fo94) located in the upper part of sample container. These results show that the density of the PHN1611 melt is equal to that of olivine (Fo94) at 13.1 ± 1.1 GPa and 2030 °C, and is 3.42 ± 0.03 gcm^{-3}. The errors are based on the accuracy of pressure and the equation of state of the buoyancy marker.

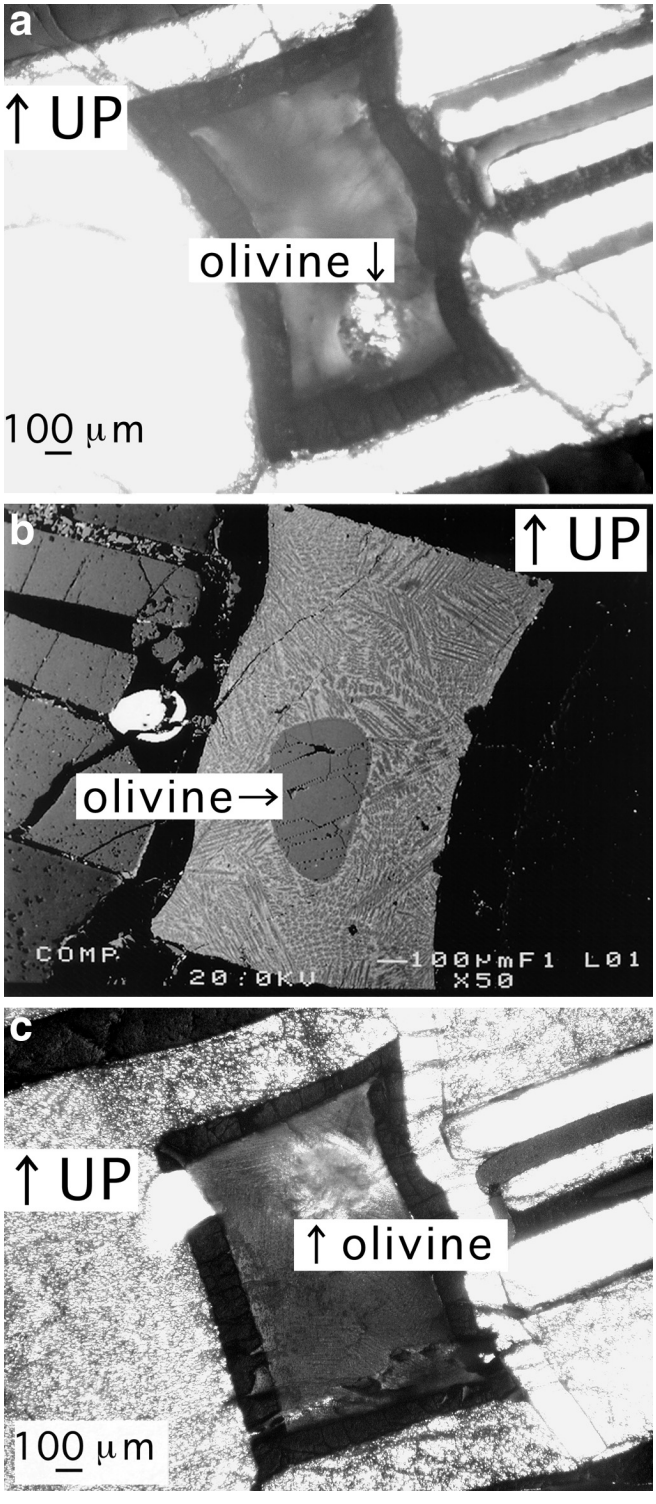

Fig. 3 a Photomicrograph of the run charge PHN-17 (sinking of olivine). **b** Backscattered image of the run charge PHN-19 (neutral buoyancy of olivine). **c** Photomicrograph of the run charge PHN-21 (flotation of olivine)

The chemical compositions of the quenched melt were measured with EPMA (Table 3). In these runs, olivine crystals were loaded as a buoyancy marker. Because of the dissolution of olivine, the chemical compositions of the quenched melts in these charges were slightly changed, as given in Table 3. However, the calculation of the zero-pressure density reveals that the change is negligible. Compositions of recovered olivines were also examined using EPMA. No chemical zoning was observed, and the compositions were Fo_{94} in all the charges. The sample container was slightly deformed. However, no movement of the density marker on squeezing was observed. In many failed experiments the surrounding silicate was partially molten in various melt fractions; however, the density marker crystals remained at the center of the sample container. We therfore believe that the crystals were loaded exactly at the center. Moreover, the experimental results show that a crystal sunk at relatively lower pressure and floated at relatively higher pressure. No exception or inconsistency was observed. Since the sample container was a tilted cylinder (Fig. 1), the sinking/floating crystals were found at the bottom/top corner.

We have observed sinking of diamond up to 20.2 GPa at 2360 °C, whereas diamond floated at 20.7 GPa (Suzuki et al. 1995). The density crossover between the PHN1611 melt and diamond is located around 20.5 GPa. The derived density of the melt is

Table 3 Chemical composition of recovered samples

	PHN-17	PHN-27	PHN-19	PHN-21
n[a]	31	29	30	30
SiO_2	44.7 (5)	45.1 (6)	44.7 (5)	44.8 (5)
Al_2O_3	2.6 (3)	2.9 (2)	1.6 (3)	2.7 (2)
FeO	9.7 (4)	9.1 (4)	9.5 (4)	9.9 (4)
MgO	39.4 (14)	40.6 (11)	40.8 (9)	39.7 (4)
CaO	3.1 (3)	2.6 (2)	2.6 (2)	3.1 (1)
Total (wt%)	99.4 (7)	100.2 (8)	99.2 (6)	100.1 (8)
Mg#[b]	88	89	88	88

[a] n number of analyses
[b] Mg# = MgO/(MgO + FeO) × 100, molar

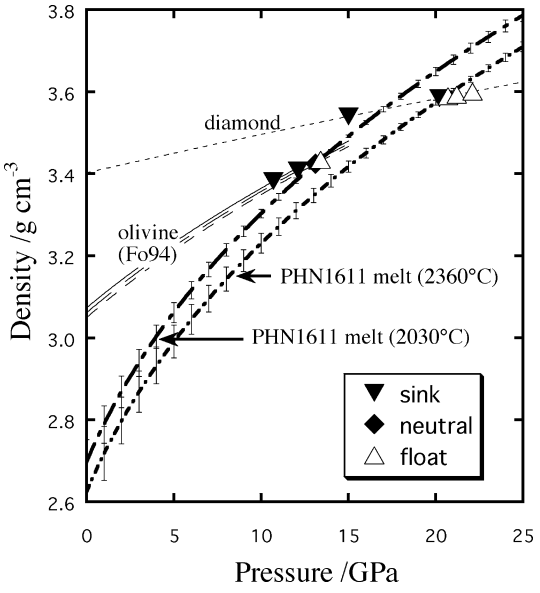

Fig. 4 Compression curves of PHN1611 melt and buoyancy markers of olivine and diamond at 2030 and 2360 °C. The density around 20 GPa is constrained by sinking/flotation of diamond in our previous study (Suzuki et al. 1995). The error on the melt is based on the calculated zero-pressure density of melt, the density of the buoyancy marker at the experimental condition, and the pressure difference between the run conditions of sinking/flotation of the buoyancy markers. Compression curves of olivine were calculated at 1870, 1950, and 2030 °C

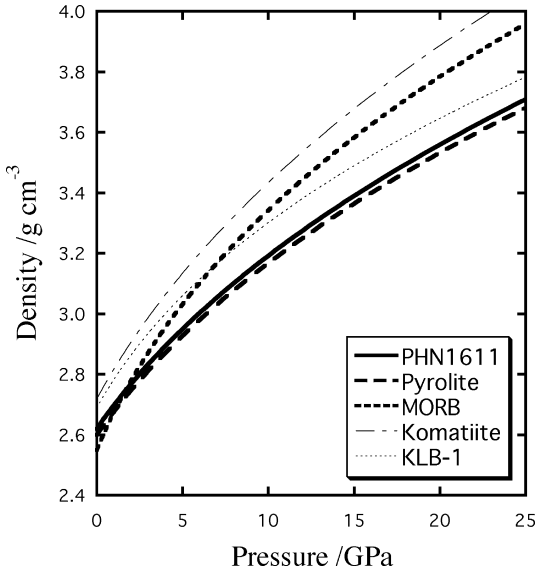

Fig. 5 Compression curves of silicate melts. PHN1611 and pyrolite at 2360 °C (this study, K = 32 GPa, K′ = 4.6); MORB at 2200 °C (Ohtani and Maeda 2001, K = 18.7 GPa, K′ = 5.0); komatiite at 1900 °C (Agee and Walker 1993, K = 26 GPa K′ = 4.25) and KLB–1 at 2000 °C (Agee and Walker 1993, K = 26 GPa, K′ 6.2)

3.59 ± 0.03 gcm^{-3} at 20.5 GPa and 2360 °C. The partial molar volume gives the zero-pressure density of $\rho_0 = 2.70 \pm 0.06$ gcm^{-3} at 2030 °C and $\rho_0 = 2.62 \pm 0.08$ gcm^{-3} at 2360 °C. We obtained results for the buoyancy test using olivine and diamond as a marker at different temperatures. Therefore, we could not determine the isothermal bulk modulus (K_T) and its pressure derivative ($K' = dK/dP$) independently. However, it is possible to constrain the K–K′ relation of the PHN1611 melt. There are large uncertainties in the zero-pressure density because the partial molar volumes were determined to 1600 °C (Lange and Carmichael 1987) and extrapolated to the experimental conditions. Therefore, a large uncertainty exists in the bulk modulus (K_0). Assuming that the temperature dependence of the bulk modulus (dK/dT) is negligible, a compression curve of PHN1611 is calculated. The bulk modulus and its pressure derivative are determined to be K = 32(3) GPa and K′ = 4.6(6), respectively. Compression curves of the PHN1611 melt, olivine (Fo94), and diamond are shown in Fig. 4.

We carried out a buoyancy test of olivine (Fo94) in pyrolite melt. The chemical composition and experimental results are given in Tables 1 and 2, respectively. We have observed sinking of Bultfontein olivine (Fo94) at 8.1 and 10.3 GPa (Ohtani et al. 1995). Pressure conditions in the work by Ohtani et al. (1995) are corrected using the revised calibration curve (Suzuki et al. 1998; Asahara and Ohtani 2001). Diamond was neutrally buoyant in the pyrolite melt at 22.1 GPa and 2360 °C. In the recovered run charge, melting of pyrolite was proved by a backscattered image; however, diamond did not move by the melting of the surrounding silicate for 300 s. In the previous studies we showed that the neutral buoyancy of crystal could constrain the density of melt. Five results of neutral buoyancy were obtained between sinking and flotation of the density marker (Ohtani et al. 1998; Suzuki et al. 1998). From these results, density of pyrolite melt is less than 3.29 gcm^{-3} at 10.3 GPa and 2000 °C, and is 3.60 ± 0.02 gcm^3 at 22.1 GPa and 2360 °C. Buoyancy experiments were also performed using primitive peridotite liquid (JPP; Table 1). Chemical compositions show that Mg# of JPP is the largest in three terrestrial peridotites. We observed sinking of diamond to 22.1 GPa, which means that the density of the melt is less than 3.60 gcm^{-3} at 22.1 GPa and 2360 °C. Compression curves of these peridotitic melts at 2360 °C are summarized in Fig. 5. The compression curve of the JPP melt is estimated to locate below that of the pyrolite melt because of the sinking of diamond at 22.1 GPa. From density measurements in the present study, it is estimated that the compressibility of peridotitic melts is similar and that density depends only on the FeO/MgO ratio in the peridotitic compositions. In Fig. 5, the pressure derivative of the bulk modulus (K′) of the pyrolite melt is assumed to be the same as that of the PHN1611 melt. The density of the MORB melt was recently measured by Ohtani and Maeda (2001) using the same method as the present study. Compression curves of komatiite and KLB-1 peridotite melt are also shown (Agee and Walker 1993). It is shown that peridotitic melt is less compressible than MORB and

komatiite. Comparing the chemical compositions of these silicates, MORB contains a higher amount of network-forming components such as SiO_2 and Al_2O_3. Since densification of silicate is believed to be due to the structural change of the silicate melt by compression (especially polyhedra of silicon and aluminum), the difference in compressibility between basaltic and peridotitic melts would be explained by the difference in the amount of compressible linkage of SiO_n and AlO_n polyhedra. A recent study of molecular dynamics simulation of aluminosilicate melt shows that the coordination number of aluminum increases with increasing pressure (e.g., Bryce et al. 1999; Suzuki et al. 2002). Bond-angle analysis of melt shows that Si–O–Si and Al–O–Si linkages in network bend, and O–Si–O and O–Al–O angles in polyhedra decrease with pressure (Suzuki et al. 2002). Even in the case of depolymerized melt such as the peridotitic melt, intrapolyhedral angles (O–Si–O and O–Al–O) can be distorted by compression. Molecular dynamics simulations of basic to ultrabasic melt have been carried out at high pressure and high temperature (e.g., Kubicki and Lasaga 1991; Wasserman et al. 1993; Matsui 1996, 1998). Matsui (1996) showed that coordination number of silicon in $CaMgSi_2O_6$ melt increases with increasing pressure. Coordination changes by compression have been also observed in $MgSiO_3$ glass and melt (Kubicki and Lasaga 1991; Wasserman et al. 1993; Matsui 1998). Molecular dynamics simulation of $MgSiO_3$ glass has revealed that both Si–O–Si and O–Si–O angles decrease with pressure, and Si–O–Si angles are more deformable than O–Si–O angles (Kubicki and Lasaga 1991). Therefore, pressure-induced densification of silicate melt is strongly related to the deformation of inter- and intralinkages of the silicon and aluminum polyhedra.

Figure 4 shows the isothermal compression curve of the PHN1611 melt at 2030 and 2360 °C. Olivine is the liquidus phase up to 13 GPa in KLB-1 (Zhang and Herzberg 1994). Ito and Takahashi (1987) reported that olivine is the liquidus phase up to 15 GPa in the PHN1611 composition. The liquidus phase is converted to modified spinel and majorite between 15 and 20 GPa. Agee and Walker (1993) estimated that the density crossover between peridotite melt and the equilibrium olivine locates at around 11 GPa. They observed sinking and flotation of forsterite and sinking of San Carlos olivine in KLB-1 peridotite melt, but they did not use olivine in equilibrium with KLB-1 melt. The present study shows that the density crossover between PHN1611 melt and the equilibrium olivine does not occur at least up to 12.3 GPa, but is clearly observed at 13.9 GPa. Density measurements of the FeO-rich peridotite melt were carried out by Ohtani et al. (1993) and Suzuki et al. (1998). The chemical composition of the FeO-rich peridotite (MA) is also shown in Table 1. The composition of olivine which is in equilibrium with the MA melt is Fo90. It has been shown that the density crossover between the melt and the equilibrium olivine occurred at around 7 GPa. MA is a model composition of the Martian mantle (Morgan and Anders 1979). It has been proposed that the density crossover between olivine and mantle melt exists at around 600 km depth in the Martian mantle (Ohtani et al. 1993; Suzuki et al. 1998). The present study implies that olivine flotation might occur within a limited depth interval of 400–450 km in the terrestrial mantle within a magma ocean.

Melting experiments of KLB-1 peridotite showed that the FeO content in the liquid on the solidus increased with increasing pressure and became close to 15 wt% over 6 GPa (Herzberg and Zhang 1996). Such an FeO-rich melt is significantly denser than the whole melt of mantle peridotite under the same P–T conditions. The density measurement of melts in the present and previous studies shows that the density inversion between silicate melt and olivine occurs at lower pressure, if the FeO/MgO ratio of melt is higher (see also Suzuki et al. 1995, 1998). Therefore, the densities of the partial melt and the surrounding olivine are estimated to be balanced at shallower depth than those of the whole melt of terrestrial mantle.

Revenaugh and Spikin (1994) reported an decrease in impedance above the 410 km discontinuity and suggested the existence of the trapped melt in this region. The present and previous studies suggest that melt can be trapped above the 410-km discontinuity because of the density crossover. The present geotherm is about 500 K lower than the dry solidus (Herzberg and Zhang 1996). Thus, the melt formed under the wet condition could explain the low impedance at around 410 km. Litasov and Ohtani (2002) recently determined the melting relation of the wet peridotite up to the top of the lower mantle condition and found a depression of the wet solidus at the base of the upper mantle associated with the olivine–wadsleyite transformation. They suggested dehydration melting of the wet mantle plume at the base of the upper mantle. Litasov and Ohtani (2002) also showed that melt formed under the wet condition at this depth has an ultramafic composition similar to that formed under dry melting. The density crossover between the wet ultramafic melt and the solid might exist at the base of the upper mantle, since water is highly compressible, based on molecular dynamics calculation (e.g., Belonoshko and Saxena 1991). However, we need further detailed experiments on the measurement of the density of the wet ultamafic melt at high pressure in order to confirm the density crossover in the present mantle.

Acknowledgements The authors thank Y. Ito for EPMA analysis. This work was partially supported by the grant-in-aid for scientific research on priority area B of the Ministry of Education, Culture, Sports, Science and Technology (no. 12126201) to E.O.

References

Abe Y, Matsui T (1985) The formation of an impact-generated H_2O atmosphere and its implications for the early thermal history of the Earth. J Geophys Res 90: C545–C559

Agee CB, Walker D (1988a) Static compression and olivine flotation in ultrabasic silicate liquid. J Geophys Res 93: 3437–3449

Agee CB, Walker D (1988b) Mass balance and phase density contrasts on early differentiation of chondritic mantle. Earth Planet Sci Lett 90: 144–156
Agee CB, Walker D (1993) Olivine flotation in mantle melt. Earth Planet Sci Lett 114: 315–324
Asahara Y, Ohtani E (2001) Melting relations of the hydrous primitive mantle in the CMAS–H_2O system at high pressure and temperatures, and implications for generation of komatiites. Phys Earth Planet Inter 125: 31–44
Belonoshko A, Saxena S (1991) A molecular dynamics study of the pressure–volume–temperature properties of super-critical fluids: I. H_2O. Ceochim Cosmochim Acta 55: 381–387
Bryce JG, Spera FJ, Stein DJ (1999) Pressure dependence of self-diffusion in the $NaAlO_2$-SiO_2 system: compositional effects and mechanisms. Am Mineral 84: 345–356
Hayashi C, Nakazawa K, Mizuno H (1979) Earth's melting due to the blanketing effect of the primordial dense atmosphere. Earth Planet Sci Lett 43: 22–28
Herzberg C, Zhang J (1996) Melting experiments on anhydrous peridotite KLB–1: compositions of magmas in the upper mantle and transition zone. J Geophys Res 101: 8271–8295
Ito E, Takahashi E (1987) Melting of peridotite at uppermost lower-mantle conditions. Nature 328: 514–517
Jagoutz E, Palme H, Baddenhausen H, Blum K, Cendales M, Dreibus G, Spettel B, Lorentz V, Wänke H (1979) The abundances of major, minor and trace elements in the Earth's mantle as derived from primitive ultramafic nodules. Proceedings 10th Lunar Planet Science Conference 2031–2050
Kaula WM (1979) Thermal evolution of Earth and Moon growing by planetesimal impacts. J Geophys Res 84: 999–1008
Kawai N, Endo S (1970) The generation of ultrahigh hydrostatic pressures by a split sphere apparatus. Rev Sci Instrum 41: 1178–1181
Kawai N, Togaya M, Onodera A (1973) A new device for pressure vessels. Proc Jpn Acad 49: 623–626
Knittke E, Wentzcovitch RM, Jeanloz R, Cohen ML (1989) Experimental and theoretical equation of state of cubic boron nitride. Nature 337: 349–351
Kubicki JD, Lasaga AC (1991) Molecular dynamics simulations of pressure and temperature effects on $MgSiO_3$ and Mg_2SiO_4 melts and glasses. Phys Chem Miner 17: 661–673
Lange RL, Carmichael ISE (1987) Densities of Na_2O–K_2O–CaO–MgO–FeO–Fe_2O_3–Al_2O_3–TiO_2–SiO_2 liquids: new measurements and derived partial molar properties. Geochim Cosmochim Acta 51: 2931–2946
Lange RL, Carmichael ISE (1990) Thermodynamic properties of silicate liquids with emphasis on density, thermal expansion and compressibility. In Nicholls J, Russel JK (eds) Modern methods of igneous petrology: understanding magmatic processes. Rev Mineral 24: 25–64
Li J, Agee CB (1996) Geochemistry of mantle–core differentiation at high pressure. Nature 381: 686–689
Li J, Agee CB (2001) The effect of pressure, temperature, oxygen fugacity and composition on partitioning of nickel and cobalt between liquid Fe–Ni–S alloy and liquid silicate: implications for the Earth's core formation. Geochim Cosmochim Acta 65: 1821–1832
Litasov K, Ohtani E (2002) Phase relations and melt compositions in CMAS–pyrolite–H_2O system up to 25 GPa. Phys Earth Planet Inter 134: 105–127
Liu J, Toper L, Zhang J, Nabrotsky A, Liebermann RC (1996) Calorimetric study of the coesite–stishovite transformation and calculation of the phase boundary. Phys Chem Miner 23: 11–16
Matsui M (1996) Molecular dynamics simulation of structures, bulk moduli, and volume thermal expansivities of silicate liquids in the system CaO–MgO–Al_2O_3–SiO_2. Geophys Res Lett 23: 395–398
Matsui M (1998) Computational modeling of crystals and liquids in the system Na_2O–CaO–MgO–Al_2O_3–SiO_2. In: Yagi T, Manghnani MH (eds) Properties of Earth and planetary materials at high pressure and temperature. American Geophysical Union, Washington DC, pp 145–151
Melosh HJ (1990) Giant impacts and the thermal state of the early Earth. In: Newsom HE, Jones JH (eds) Origin of the Earth. Oxford University Press, New York, pp 69–83,
Miller GH, Stolper EM, Ahrens TJ (1991a) The equation of state of a molten komatiite 2. Application to komatiite petrogenesis and the Hadean mantle. J Geophys Res 96: 11849–11864
Miller GH, Stolper EM, Ahrens TJ (1991b) The equation of state of a molten komatiite 1. Shock wave compression to 36 GPa. J Geophys Res 96: 11831–11848
Morgan JW, Anders E (1979) Chemical composition of Mars. Geochim Cosmochim Acta 43: 1601–1610
Morishima H, Kato T, Suto M, Ohtani E, Urakawa S, Utsumi W, Shimomura O, Kikegawa T (1994) The phase boundary between α- and β-Mg_2SiO_4 determined by in situ X-ray observation. Science 265: 1202–1203
Nisbet EG, Walker D (1982) Komatiites and the structure of the Archaean mantle. Earth Planet Sci Lett 60: 105–113
Nixon PH, Boyd FR (1973) Petrogenesis of the granular and sheared ultrabasic nodule suite in kimberlites. In: Nixon PH (eds) Lesotho kimberlites. Lesotho National Development, Maseru, pp 48–56
O'Hara MJ (1975) The bearing of phase equilibria studies in synthetic and natural systems on the origin and evolution of basic and ultrabasic rocks. Earth Sci Rev 4: 69–133
Ohtani E (1983) Melting temperature distribution and fractionation in the lower mantle. Phys Earth Planet Inter 33: 12–25
Ohtani E (1984) Generation of komatiite magma and gravitational differentiation in the deep upper mantle. Earth Planet Sci Lett 67: 261–272
Ohtani E (1985) The primordial terrestrial magma ocean and its implication for stratification of the mantle. Phys Earth Planet Inter 38: 70–80
Ohtani E (1988) Chemical stratification of the mantle formed by melting in the early stage of the terrestrial evolution. Tectonophysics 154: 201–210
Ohtani E (1990) Majorite fractionation and genesis of komatiites in the deep mantle. Precambrian Res 48: 195–202
Ohtani E, Maeda M (2001) Density of basaltic melt at high pressure and stability of the melt at the base of the lower mantle. Earth Planet Sci Lett 193: 69–75
Ohtani E, Suzuki A, Kato T (1993) Flotation of olivine in the peridotite melt at high pressure. Proc Jpn Acad (B) 69: 23–28
Ohtani E, Suzuki A, Kato T (1998) Flotation of olivine and diamond in mantle melt at high pressure: implications for fractionation in the deep mantle and ultradeep origin of diamond. In: Manghnani MH, Yagi T (eds) Properties of Earth and planetary materials at high pressure and temperature. Geophysical Monograph. 101, American Geophysical Union, Washington DC, pp 227–239
Ohtani E, Yurimoto H, Seto S (1997) Element partitioning between metallic liquid, silicate liquid, and lower-mantle minerals: implications for core formation of the Earth. Phys Earth Planet Inter 100: 97–114
Ohtani E, Nagata Y, Suzuki A, Kato T (1995) Melting relations of peridotite and the density crossover in planetary mantles. Chem Geol 120: 207–221
Onodera A (1987) Octahedral-anvil high-pressure devices. High Press High Temp 19: 579–609
Revenaugh J, Sipkin SA (1994) Seismic evidence for silicate melt atop the 410-km mantle discontinuity. Nature 369: 474–476
Ringwood AE (1975) Composition and petrology of the Earth' s mantle. McGraw-Hill, New York
Sasaki S, Nakazawa K (1986) Metal-silicate fractionation in the growing Earth: energy source for the terrestrial magma ocean. J Geophys Res 91: 9231–9238
Susaki J, Akaogi M, Akimoto S, Shimomura O (1985) Garnet-perovskite transition in $CaGeO_3$: In-situ X-ray measurements using synchrotron radiation. Geophys Res Lett 12: 729–732
Suzuki A, Ohtani E, Kato T (1995) Flotation of diamond in mantle melt at high pressure. Science 269: 216–218
Suzuki A, Ohtani E, Kato T (1998) Density and thermal expansion of a peridotite melt at high pressure. Phys Earth Planet Inter 107: 53–61

Suzuki A, Ohtani E, Funakoshi K, Terasaki H, Kubo T (2002) Viscosity of albite melt at high pressure and high temperature. Phys Chem Miner 29: 159–165

Takahashi E (1986) Melting of a dry peridotite KLB-1 up to 14 GPa: implications on the origin of peridotitic upper mantle. J Geophys Res 91: 9367–9382

Wasserman EA, Yuen DA, Rustad JR (1993) Molecular dynamics study of the transport properties of perovskite melts under high-temperature and –pressure conditions. Earth Planet Sci Lett 114: 373–384

Yasuda A, Fujii T, Kurita K (1994) Melting phase relations of an anhydrous mid-ocean ridge basalt from 3 to 20 GPa: implications for the behavior of subducted oceanic crust in the mantle. J Geophys Res 99: 9401–9414

Zhang J, Herzberg C (1994) Melting experiments on anhydrous peridotite KLB-1 from 5.0 to 22.5 GPa. J Geophys Res 99: 17729–17742